

# Artificial Neural Network-Based Gain-Scheduled State Feedback Speed Controller for Synchronous Reluctance Motor

Research Paper

Tomasz Tarczewski<sup>1,\*</sup>, Łukasz J. Niewiara<sup>1</sup>, Lech M. Grzesiak<sup>2</sup>

<sup>1</sup>Institute of Engineering and Technology, Faculty of Physics, Astronomy and Informatics, Nicolaus Copernicus University in Toruń, Toruń, Poland

<sup>2</sup>Institute of Control and Industrial Electronics, Warsaw University of Technology, Warsaw, Poland

Received: October 12, 2021; Accepted: November 10, 2021

**Abstract:** This paper focuses on designing a gain-scheduled (G-S) state feedback controller (SFC) for synchronous reluctance motor (SynRM) speed control with non-linear inductance characteristics. The augmented model of the drive with additional state variables is introduced to assure precise control of selected state variables (i.e. angular speed and  $d$ -axis current). Optimal, non-constant coefficients of the controller are calculated using a linear-quadratic optimisation method. Non-constant coefficients are approximated using an artificial neural network (ANN) to assure superior accuracy and relatively low usage of resources during implementation. To the best of our knowledge, this is the first time when ANN-based gain-scheduled state feedback controller (G-S SFC) is applied for speed control of SynRM. Based on numerous simulation tests, including a comparison with a signum-based SFC, it is shown that the proposed solution assures good dynamical behaviour of SynRM drive and robustness against  $q$ -axis inductance, the moment of inertia and viscous friction fluctuations.

**Keywords:** synchronous reluctance motor • state feedback controller • gain-scheduling • artificial neural network • robustness analysis

## 1. Introduction

High torque density, robust design and low manufacturing cost have caused synchronous reluctance motors (SynRMs) to recently receive increased attention (Farhan et al., 2020). As stated in Boldea and Tutelea (2018), SynRMs are even 20% cheaper and 4% more efficient than induction motors in the field of variable-speed drives. For this reason, this type of motor is recently applied in electric vehicles, elevators, chillers and HVAC systems (Bianchi et al., 2016; Credo et al. 2020; Oliveira and Ukil 2019; Li et al., 2020).

The advantages of SynRM mentioned above come with non-linear inductance characteristics (Farhan et al., 2020; Boldea and Tutelea 2018). Such shortcoming causes the need for advanced control algorithms to achieve high dynamic performance. Several publications concerning non-linear control approaches are available in the literature. In Senjyu et al. (2003), a high-efficiency control strategy based on an extended Kalman filter (EKF) is proposed to improve machine efficiency. The EKF is used to estimate the inductance and resistance of the SynRM. These are used to modify the parameters of controllers that operate in a cascade manner. Such a solution ensures better efficiency when compared with conventional control methods. However, the tuning process of the EKF and cascade controllers with non-constant gains is not trivial. In Hadla and Cruz (2016), a control structure with finite control set model predictive controller with the outer PI speed controller is proposed. The active flux predictive control is developed to assure fast torque response and ripple minimisation. Reduced cross-coupling effects and suitable dynamic responses are obtained for robust control based on linear matrix inequalities (Scalcon et al., 2020). In this solution, expert knowledge is required as the synthesis process of the controller is based on the Lyapunov approach.

\* Email: lukniewiara@umk.pl

Artificial intelligence-based control methods can also be applied to cope with the non-linear and cross-coupled behavior of electrical drives (Cvetkovski and Petkovska 2021, Ewert 2019). In Lin et al. (2019), an adaptive backstepping speed controller is designed. In order to improve the transient dynamic response of SynRM under maximum torque per ampere (MTPA) operating conditions, a recurrent Hermite fuzzy neural network is used. Thanks to applying the artificial intelligence-based approach, a higher current angle command for the transient torque results in faster dynamic response of the SynRM. Due to this, drawbacks of the classical PI control structure have been overcome. By contrast, designing a control system with a recurrent Hermite fuzzy neural network seems to be not trivial as it is difficult to adjust the fuzzy rules and membership functions online. The presented results indicate that the described solution assures robustness and satisfactory speed control performance. In Truong et al. (2016), an adaptive approach based on artificial neural networks (ANNs) is used to calculate the optimal stator currents of SynRM. The Adaline with an online learning process (i.e. the Widrow–Hoff algorithm) is utilised. Designed Adaline controllers take the place of the conventional torque and speed ones. The presented results show the reduction of torque and speed ripples and better convergence; the copper losses have also been reduced.

As shown in Tarczewski et al. (2021) and Hannoun et al. (2011), a gain-scheduled (G-S) approach can also be applied to cope with the non-linear and cross-coupled behaviour of SynRM. In Hannoun et al. (2011), a PI current controller with variable gains is proposed, while in Tarczewski et al. (2021), a cascade-free state feedback controller (SFC) is applied for simultaneous control of motor's current and speed. However, in Hannoun et al. (2011), a state feedback approach is also utilised to synthesise the self-tuned PI current controller. Its parameters are adjusted online in relation to the current and position change. In addition, a back-EMF compensation scheme has been implemented to reduce the bandwidth requirements placed upon the controller. As a result, the controller limits the loop bandwidth variations due to the gain changing. The results prove the good performance of this type of regulation.

The non-linearity tolerance and robustness shows SFC to be a good alternative for complex control schemes developed for SynRM (Tarczewski et al., 2021; Brasel 2014; Safonov and Athans 1977; Shyu et al., 2001; Tarczewski and Grzesiak 2009). The provisional results shown in Tarczewski et al. (2021) indicate that high-performance speed control of SynRM can be obtained if a gain-scheduled state feedback controller (G-S SFC) is used. For this reason, it was decided to perform further investigations of this solution. In Tarczewski et al. (2021), the non-constant coefficients of the controller are implemented using the lookup table (LUT)-based approach, where a relatively large amount of the memory resources is used to assure satisfactory accuracy. As ANNs can be applied to approximate non-constant relationships with superior accuracy (Grzesiak and Tarczewski 2015), it was decided to design and investigate the behaviour of ANN G-S SFC. Numerical tests were performed in terms of (i) precise control of angular velocity and  $d$ -axis current and (ii) robustness against  $q$ -axis inductance, the moment of inertia, and viscous friction uncertainties.

This paper is organised as follows. Section II describes a model of the SynRM drive with respect to simplifying assumptions. In Section III, ANN-based G-S SFC is presented, and the training process of the ANN gain approximator is shown. Section IV discusses numerical tests, including the behavior of angular velocity and  $d$ -axis current control and robustness against  $q$ -axis inductance and mechanical parameters fluctuations. A comparison of the proposed ANN-based G-S SFC with signum-based SFC is also included. Section V concludes this paper.

## 2. SynRM Drive's Model

In this section, a model of the SynRM drive is introduced. Since an SFC responsible for cascade-free control of motor currents and angular velocity is to be designed, it was decided to express the model of the plant in a state equation form. For convenient development of vector control, it is described in the  $d$ - $q$  reference frame (Kazmierkowski et al., 2001). A schematic diagram of the considered control structure is shown in Figure 1.

Because of the complexity of the considered model, a few assumptions are made to simplify the designing process of the controller and assure high-performance operation of the drive (Tarczewski et al., 2021) as follows:

- Magnetic saturation of inductance is considered for  $d$ -axis, that is,  $L_d(i_d)$  is taken into account (Boldea and Tutelea 2018; Awan et al., 2019);
- A constant value of  $L_q$  is assumed (Boldea and Tutelea 2018; Kazmierkowski et al. 2011; Yousefi-Talouki et al., 2017);
- The decoupling procedure is applied to remove cross-coupling between the  $d$ - and  $q$ -axes introduced by the back-EMFs (Kazmierkowski et al. 2011; Tarczewski et al., 2021);

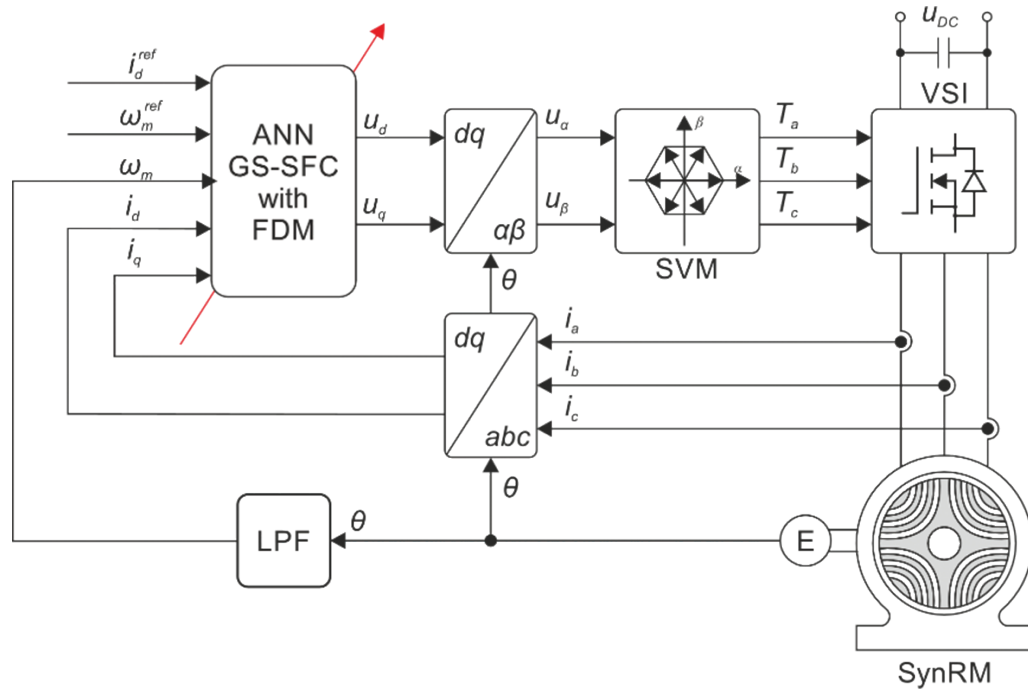


**Fig. 1.** Schematic diagram of SynRM control structure with ANN-based G-S SFC. ANN, artificial neural network; G-S SFC, gain-scheduled state feedback controller; SynRM, synchronous reluctance motor.

- Additional state variables are introduced to provide steady-state error-free control of the  $d$ -axis current and the angular velocity (Tarczewski et al., 2021);
- The load torque is omitted during the synthesis process of the controller.

For the assumptions listed above, the following model of the SynRM drive is obtained (Tarczewski et al., 2021):

$$\frac{d\mathbf{x}}{dt} = \mathbf{A}(L_d, i_d)\mathbf{x}(t) + \mathbf{B}(L_d)\mathbf{u}(t) + \mathbf{F}\mathbf{r}(t) \quad (1)$$

with:

$$\mathbf{A}(L_d, i_d) = \begin{bmatrix} -\frac{R_s}{L_d(i_d)} & 0 & 0 & 0 & 0 \\ 1 & 0 & 0 & 0 & 0 \\ 0 & 0 & -\frac{R_s}{L_q} & 0 & 0 \\ 0 & 0 & \frac{3p(L_d(i_d) - L_q)i_d}{2J_m} & -\frac{B_m}{J_m} & 0 \\ 0 & 0 & 0 & 1 & 0 \end{bmatrix}, \quad \mathbf{B}(L_d) = \begin{bmatrix} \frac{K_p}{L_d(i_d)} & 0 \\ 0 & 0 \\ 0 & \frac{K_p}{L_q} \\ 0 & 0 \\ 0 & 0 \end{bmatrix}, \quad \mathbf{F} = \begin{bmatrix} 0 & 0 \\ -1 & 0 \\ 0 & 0 \\ 0 & 0 \\ 0 & -1 \end{bmatrix}, \quad \mathbf{x}(t) = \begin{bmatrix} i_d(t) \\ e_i(t) \\ i_q(t) \\ \omega_m(t) \\ e_\omega(t) \end{bmatrix},$$

$$\mathbf{u}(t) = \begin{bmatrix} u_{dc}(t) \\ u_{qc}(t) \end{bmatrix}, \quad \mathbf{r}(t) = \begin{bmatrix} i_d^{ref}(t) \\ \omega_m^{ref}(t) \end{bmatrix}$$

where  $R_s$  – stator resistance,  $L_d(i_d)$ ,  $L_q$  – stator inductances,  $P$  – number of pole pairs,  $B_m$  – viscous friction,  $J_m$  – moment of inertia,  $K_p$  – converter gain,  $i_d(t)$ ,  $i_q(t)$  – space vector current components,  $\omega_m(t)$  – angular velocity,

$u_{dc}(t), u_{qc}(t)$  – decoupled space vector voltage components and  $e_i(t)$  – state variable corresponds to the integral of the  $d$ -axis current error:

$$e_i(t) = \int_0^t [i_d(\tau) - i_d^{ref}(\tau)] d\tau \quad (2)$$

$e_\omega(t)$  – state variable corresponds to the integral of the angular velocity error:

$$e_\omega(t) = \int_0^t [\omega_m(\tau) - \omega_m^{ref}(\tau)] d\tau \quad (3)$$

$i_d^{ref}(\tau)$  – the reference value of  $d$ -axis current,  $\omega_m^{ref}(\tau)$  – the reference value of angular velocity. From Eq. (1), it can be seen that cross-couplings between  $d$  and  $q$  axes do not exist. These were removed using a feedback decoupling method. In this approach, additional voltage components consisting of cross-coupled back-EMFs are introduced with respective signs to eliminate cross-coupled terms. A detailed explanation can be found in Tarczewski et al. (2021).

After analysis of the state and input matrices from Eq. (1), one can see that regardless of the FDM procedure used, dependence between  $L_d$  and  $i_d(t)$  is necessary to calculate the respective components. In this paper, the following notation has been adopted:

$$a_{11} = -\frac{R_s}{L_d(i_d)}, \quad a_{43} = \frac{3p(L_d(i_d) - L_q)}{2J_m}, \quad b_{11} = \frac{K_p}{L_d(i_d)} \quad (4)$$

and the coefficients mentioned above were calculated for SynRM from ABB (type M3AL 90LA 4 IMB3/IM1001) with the parameters listed in Table 1.

Based on the motor parameters, the relation between  $L_d$  and  $i_d(t)$  and the shape of Eq. (4) have been obtained, and these are shown in Figure 2.

**Table 1.** Parameters of SynRM drive

Parameter	Symbol	Value	Unit
Nominal power	$P_N$	1.1	kW
Nominal current	$I_N$	4.1	A
Stator resistance	$R_s$	6	
$q$ -axis inductance	$L_q$	40	mH
Moment of inertia	$J_m$	$2 \times 10^{-3}$	kgm <sup>2</sup>
Viscous friction	$B_m$	$1.4 \times 10^{-2}$	Nms/rad
Number of pole pairs	$p$	2	
Converter gain	$K_p$	282	

SynRM, synchronous reluctance motor.

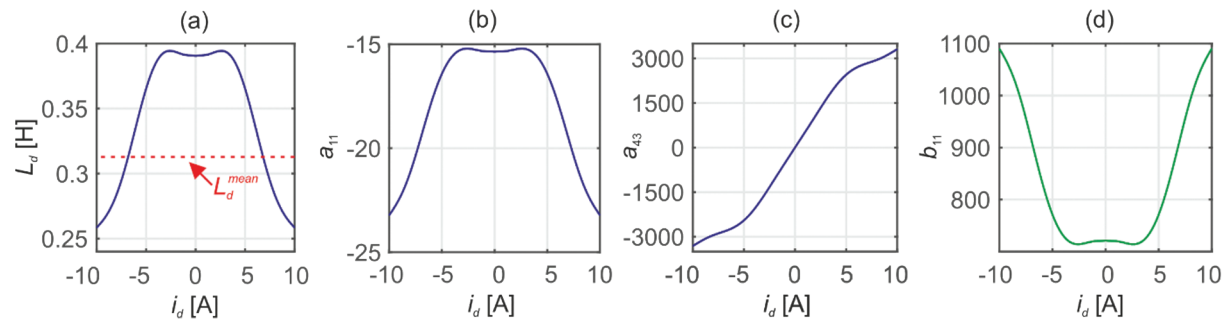


**Fig. 2.** Inductance and matrix coefficients versus  $d$ -axis current: (a)  $L_d$ , (b)  $a_{11}$ , (c)  $a_{43}$  and (d)  $b_{11}$ .

As highly non-linear relationships have been obtained, it was decided to propose a non-linear control strategy. In Figure 2(a), it can be seen the constant value of  $d$ -axis inductance. It was calculated as a mean value of the presented relationship and will be used to design SFC for comparison. Both are described in the following section.

### 3. ANN-based G-S SFC and Signum-based SFC

In this section, the design process of state feedback speed controller with non-constant coefficients is presented. Among other adaptive control schemes, the G-S SFC is relatively simple for design and implementation and assures robustness and high-performance operation of the AC motors (Tarczewski et al., 2021; Brasel 2014; Tarczewski et al., 2017). In this solution, a non-stationary model of the plant, as in Eq. (1), is applied to obtain the controller's coefficients for the actual value of  $L_d$  and  $i_d$ . In such a case, a set of SFC coefficients at the operating points defined by an actual value of  $d$ -axis current will be calculated and the following control law is introduced:

$$\mathbf{u}(t) = \mathbf{K}(i_d) \mathbf{x}(t) \quad (5)$$

with:

$$\mathbf{K}(i_d) = \begin{bmatrix} k_{d1}(i_d) & k_{d2}(i_d) & k_{d3}(i_d) & k_{d4}(i_d) & k_{d5}(i_d) \\ k_{q1}(i_d) & k_{q2}(i_d) & k_{q3}(i_d) & k_{q4}(i_d) & k_{q5}(i_d) \end{bmatrix}$$

where  $\mathbf{K}(i_d)$  is the non-constant gain matrix of SFC controller. In this approach, a linear-quadratic optimisation method has been applied to calculate the coefficients of the controller. These are selected during minimisation of the following performance index:

$$I_{LQR} = \int_0^t [\mathbf{x}^T(\tau) \mathbf{Q} \mathbf{x}(\tau) + \mathbf{u}^T(\tau) \mathbf{R} \mathbf{u}(\tau)] d\tau \quad (6)$$

where  $\mathbf{Q} = \text{diag}([q_1 \ q_2 \ q_3 \ q_4 \ q_5])$ ,  $\mathbf{R} = \text{diag}([r_1 \ r_2])$  – manually selected penalty matrices. Values of  $\mathbf{Q}$  and  $\mathbf{R}$  have been selected to provide steady-state error-free control of the angular velocity and  $d$ -axis current and good dynamical behaviour of the drive. According to the information presented in Tarczewski et al. (2021), the following coefficients were selected:  $q_1 = q_3 = q_4 = r_1 = r_2 = 1, q_2 = 1000, q_5 = 100$ . Gain coefficients have been calculated for operating points defined by the  $d$ -axis current in a range of  $i_d \in [-10; 10]$  A with 10 mA resolution. The non-constant coefficients obtained using the `lqrd` MATLAB's function are shown in Figure 3, while the rest from Eq. (5) are equal to zero.

From Figure 3., one can see that coefficients of SFC are highly non-linear, and therefore its approximation and implementation seem to be non-trivial. For the sake of comparison, a constant approximation of the coefficients also has been made. Since  $k_{q4}$  and  $k_{q5}$  coefficients are discontinuous, it was decided to apply signum-based approximation, as shown in Figure 3 (d) and (e). Therefore, the obtained controller was named a signum-based SFC. In the case of non-constant coefficients, a gain-scheduling task can be made using lookup tables or a polynomials-based approach. However, such solutions require large hardware resources for good accuracy (Tarczewski et al., 2021; Hannoun et al., 2011; Kumar et al., 2016). In the proposed approach, an ANN gain approximator is designed. As an input, the actual value of  $d$ -axis current in a range of  $i_d \in [-10; 10]$  A is used, while the output should approximate non-constant coefficients of SFC shown in Figure 3 and the  $L_d(i_d)$  relationship from Figure 2(a). For this reason, a neural network with one input and six outputs has been used. The structure of ANN used is shown in Figure 4(a), while the training process is presented in Figure 4(b).

From Figure 4(a), it can be seen that a feedforward neural network with one hidden layer has been used. A hyperbolic tangent activation function has been used in the hidden layer, while a linear function has been applied in an output one. The samples were divided for training, validation and testing sets in the following proportions:

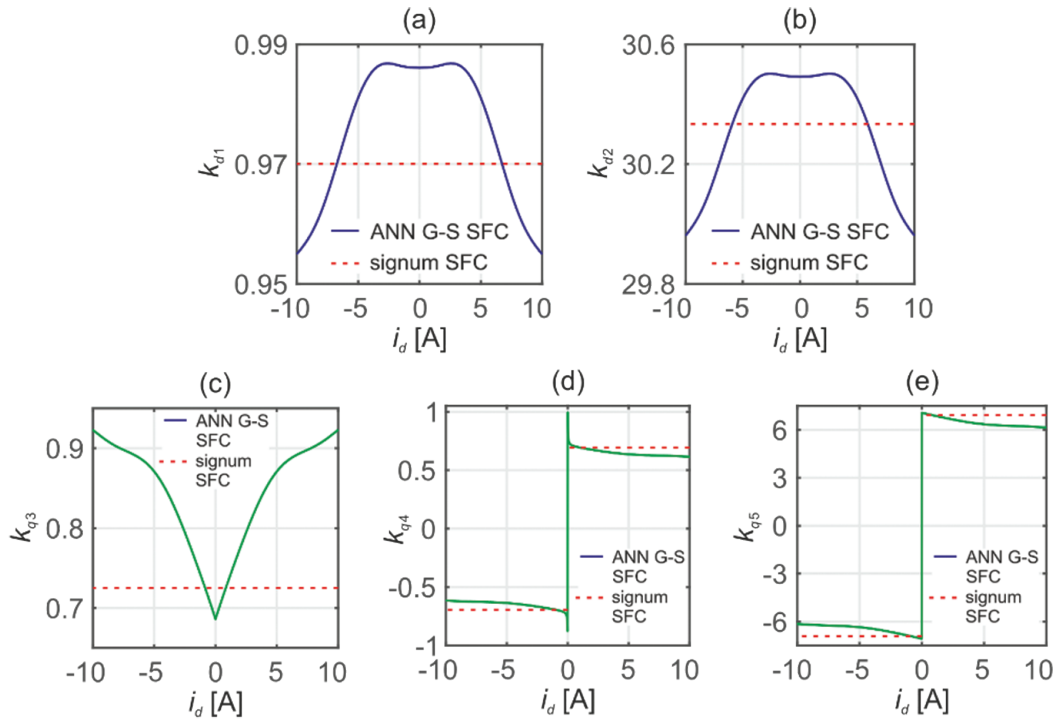


**Fig. 3.** Non-constant coefficients of SFC versus  $d$ -axis current and constant approximation: (a)  $k_{d1}$ , (b)  $k_{d2}$ , (c)  $k_{q3}$ , (d)  $k_{q4}$  and (e)  $k_{q5}$ .

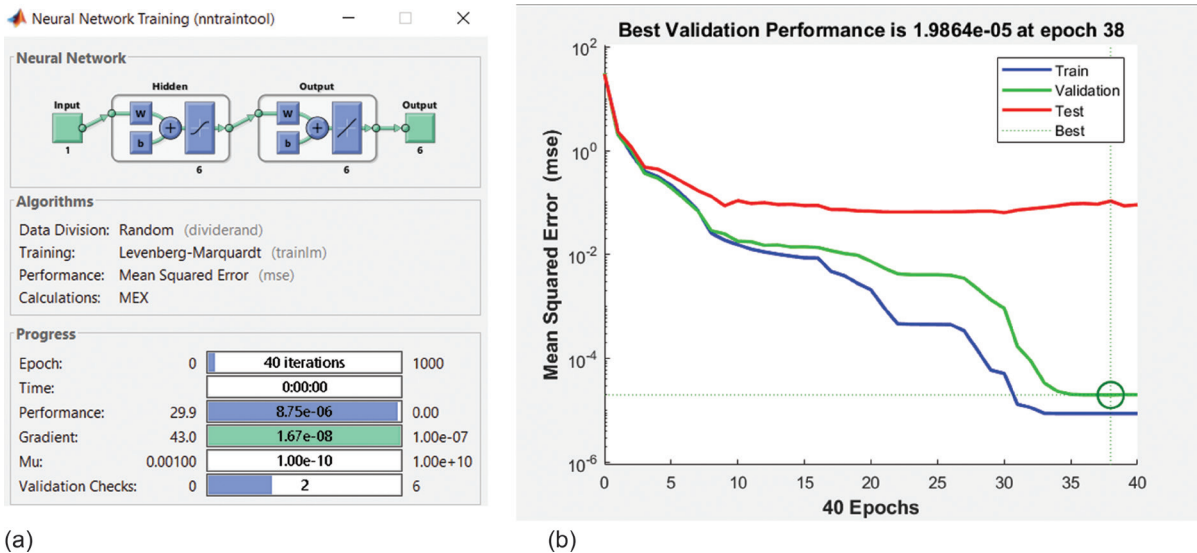


**Fig. 4.** Training stage of ANN gain approximator: (a) structure of ANN and training progress and (b) epochs. ANN, artificial neural network.

70%, 15% and 15%, to provide an efficient learning process. The Levenberg–Marquardt backpropagation algorithm has been used to learn ANN. From the recorded training process, it can be seen that a superior approximation level has been obtained for a relatively small ANN after 40 iterations. The considered task was made using nftool from MATLAB R2021a. The overall time required for neural fitting made on PC with Intel Core i7-4720 HQ CPU @ 2.6 GHz and 8 GB ram is less than 1 s. Numerical validation of the designed ANN-based G-S SFC is presented in the following section.

## 4. Numerical Experiments

The proposed control scheme has been implemented in MATLAB/Simulink, and the designed control structure is shown in Figure 5(a), the block diagram of ANN-based G-S SFC is presented in Figure 5(b), while the block diagram of signum-based SFC is depicted in Figure 5(c).

As was stated before, an ANN is applied to approximate the non-linear coefficients of SFC. Moreover, the  $d$ -axis inductance value necessary for calculating the decoupling components in FDM is also provided. From Figure 5(a), one can see that the proposed SFC allows controlling the  $d$ -axis current and the angular velocity. Due to this, various control strategies for SynRM can be implemented.

First, the complexity of the developed control algorithm has been investigated using the Simulink Profiler Tool. It was found that the execution time of the proposed approach is 60% longer compared with the LUTs-based SFC described in Tarczewski et al. (2021). On the other hand, a LUT-based solution requires a relatively large amount of memory resources to assure satisfactory accuracy. As the considered control schemes are implemented in a microcontroller with ARM Cortex 32-bit core, the complexity of the ANN-based approach seems not to be an issue.

The operation of SynRM with ANN-based G-S SFC is presented in Figure 6. An analysis of angular velocity reversal transients with 3 Nm load torque step changes in Figure 6(a) and (f) illustrates the satisfactory performance (i.e. good dynamic behaviour, zero steady-state error, and fast load torque compensation). From Figure 6(b) and (g), one can see proper  $d$ -axis current control in both directions, allowing various control strategies to be implemented. It can be seen that the rise time and the maximum fluctuation of angular speed caused by load torque step changes are shorter for the increased value of  $d$ -axis current. The same observation applies to the electromagnetic torque produced by SynRM, as shown in Figure 6(e) and (j). Finally, the sinusoidal shape of phase currents recorded

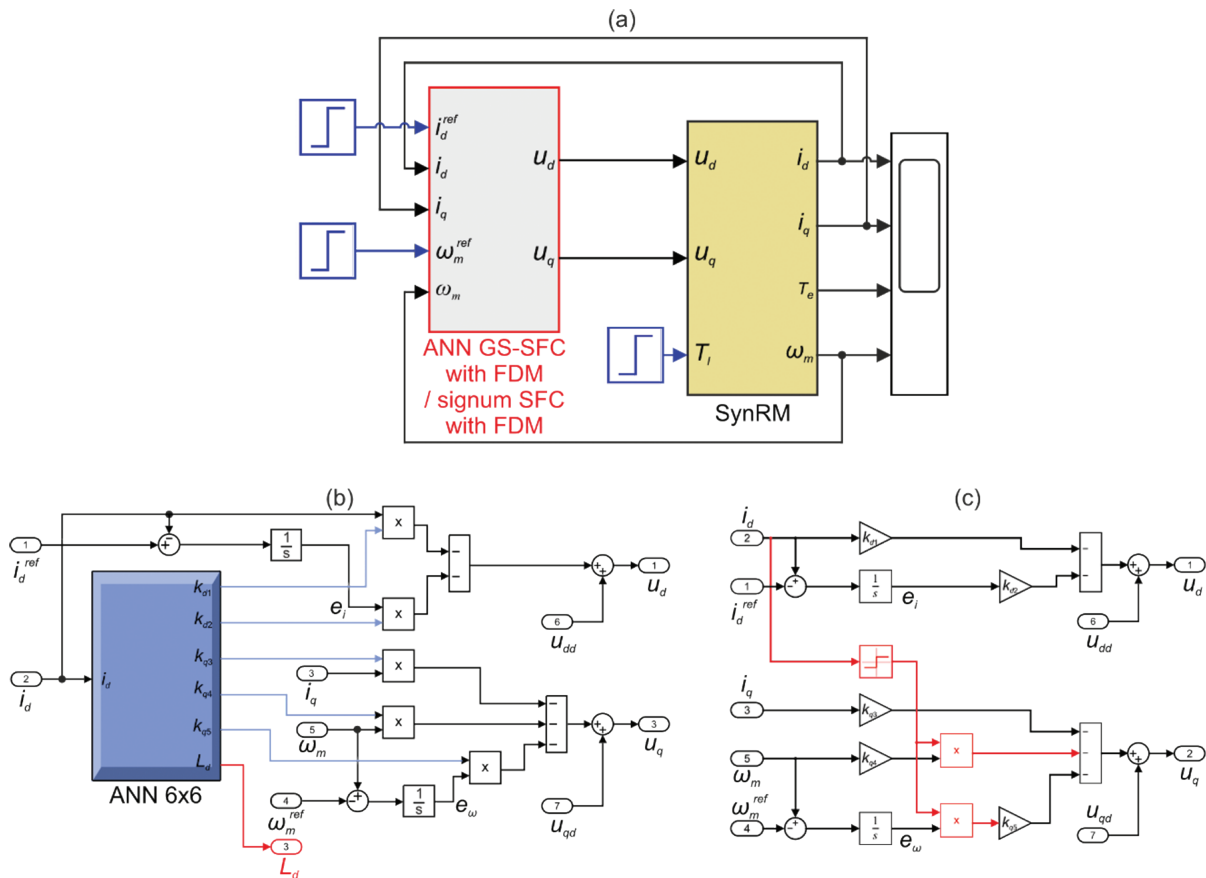


**Fig. 5.** Block diagram of (a) proposed control structure, (b) ANN-based G-S SFC and (c) signum-based SFC. ANN, artificial neural network; G-S SFC, gain-scheduled state feedback controller.

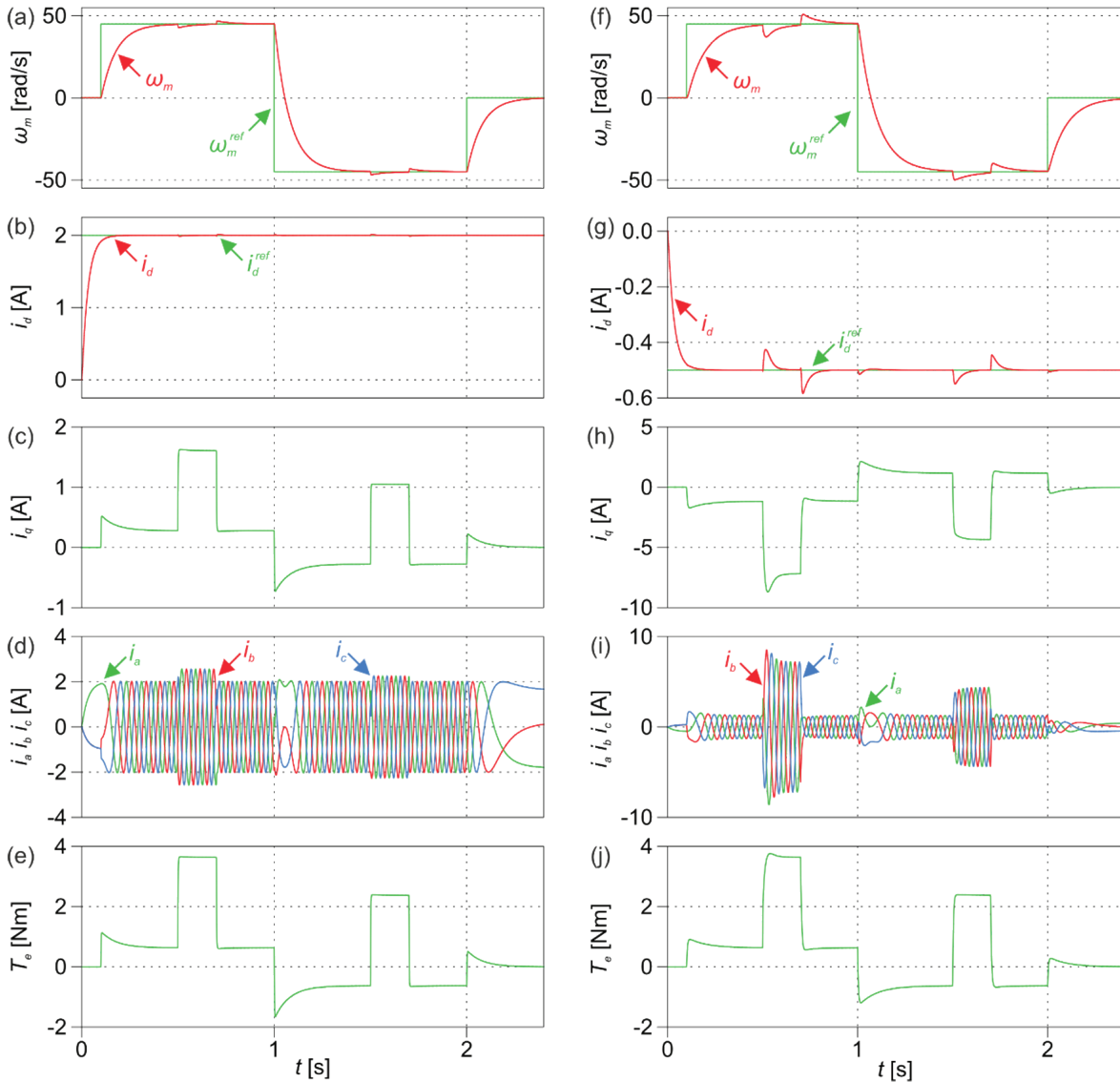


**Fig. 6.** Angular velocity reversal transients of SynRM with ANN-based G-S SFC with 3 Nm load torque perturbation for  $i_d^{ref} = 2$  A (left column) and  $i_d^{ref} = -0.5$  A (right column): (a) and (f) angular velocity, (b) and (g) direct current, (c) and (h) quadrature current, (d) and (i) phase currents, (e) and (j) electromagnetic torque. ANN, artificial neural network; G-S SFC, gain-scheduled state feedback controller; SynRM, synchronous reluctance motor.

during start-up, velocity reversal, and the load torque compensation indicates a high-performance operation of the investigated drive.

In the next step, the robustness of the proposed ANN-based G-S SFC is investigated. As the constant value of  $L_q$  has been assumed during synthesis, it was decided to investigate its impact on control performance.

From Figure 7, it can be seen that the proposed control system is robust against inductance fluctuations in the range of  $[L_q/2; 2L_q]$ . The impact of the  $L_q$  value on the angular speed and the  $d$ -axis current control is negligible. Shown in Figure 7(c) and (f), waveforms of the  $q$ -axis current indicate slight differences caused by the  $L_q$  fluctuations, especially when the load torque is imposed.

The impact of mechanical parameters fluctuation on the control system performance has been investigated in the next stage. Since the SynRM drive can be applied in an autonomous electric vehicle, robustness against mechanical parameters fluctuation (i.e. the moment of inertia and friction) was also investigated, and the respective waveforms are shown in Figure 8.

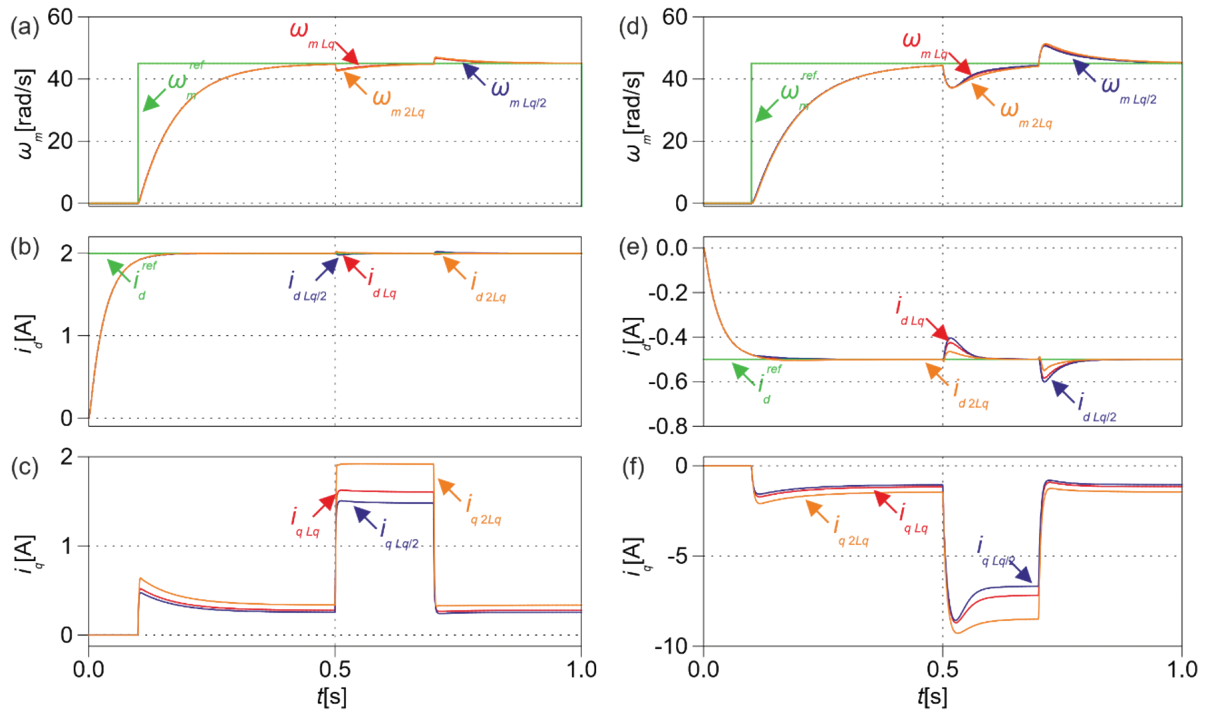


**Fig. 7.** Angular velocity reversal transients of SynRM with ANN-based G-S SFC with 3 Nm load torque perturbation for  $i_{cd}^{ref} = 2$  A (left column) and  $i_{cd}^{ref} = -0.5$  A (right column) for  $L_q$  fluctuation: (a) and (d) angular velocity, (b) and (e) direct current, (c) and (f) quadrature current. ANN, artificial neural network; G-S SFC, gain-scheduled state feedback controller; SynRM, synchronous reluctance motor.

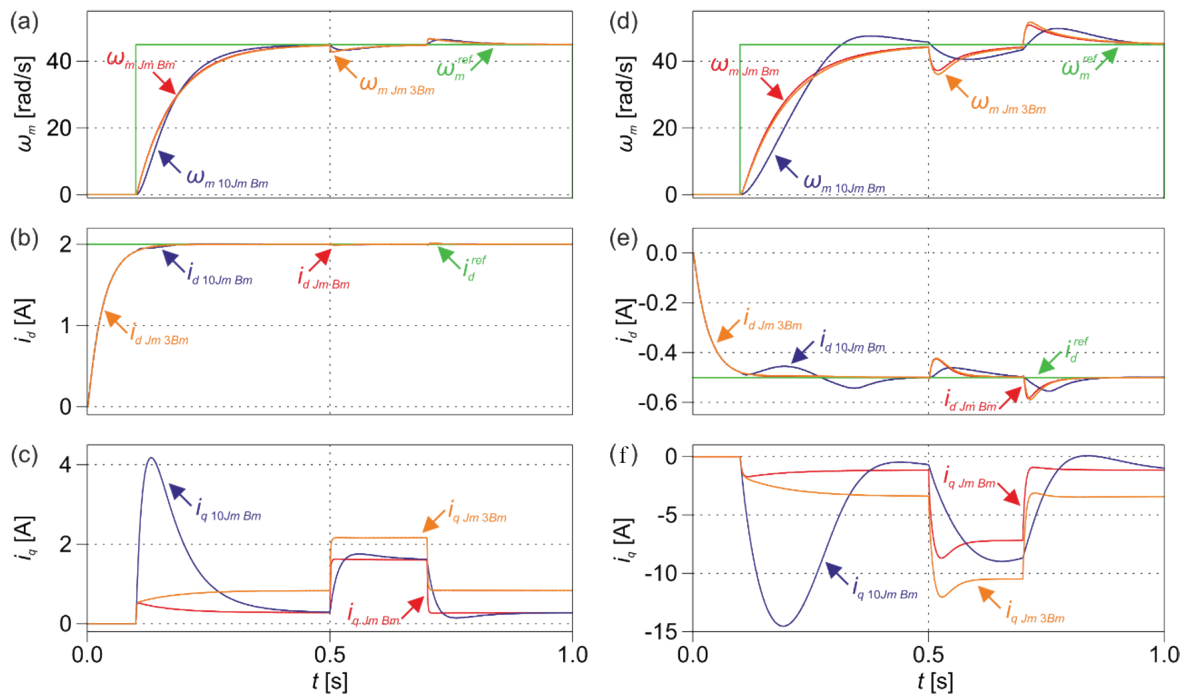


**Fig. 8.** Angular velocity reversal transients of SynRM with ANN-based G-S SFC with 3 Nm load torque perturbation for  $i_{cd}^{ref} = 2$  A (left column) and  $i_{cd}^{ref} = -0.5$  A (right column) for  $J_m$  and  $B_m$  fluctuation: (a) and (d) angular velocity, (b) and (e) direct current, (c) and (f) quadrature current. ANN, artificial neural network; G-S SFC, gain-scheduled state feedback controller; SynRM, synchronous reluctance motor.

**Table 2.** Comparison of the IAE performance for ANN-based G-S SFC index for parameters fluctuation

	$L_q, J_m, B_m$	$L_q/2, J_m, B_m$	$2L_q, J_m, B_m$	$L_q, 10J_m, B_m$	$L_q, J_m, 3B_m$
IAE for $i_d^{ref} = 2$ A	3.822	3.798	3.881	3.833	3.885
IAE for $i_d^{ref} = -0.5$ A	5.531	5.453	5.731	6.401	5.949

ANN, artificial neural network; G-S SFC, gain-scheduled state feedback controller.

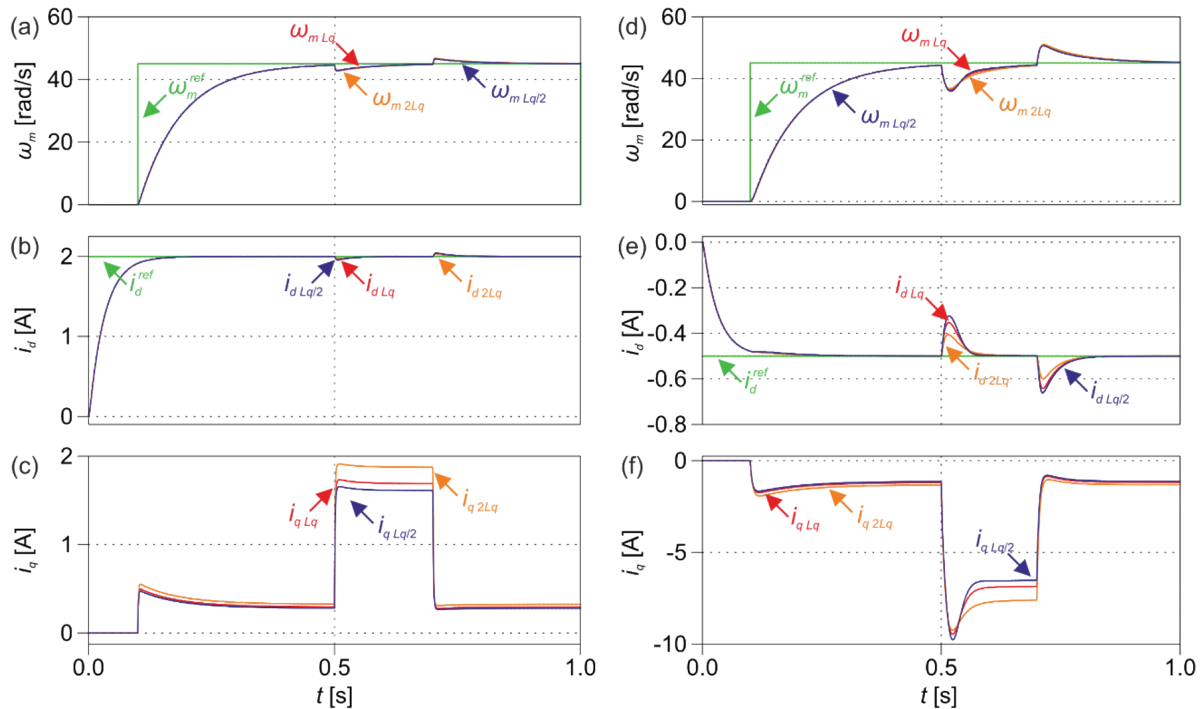


**Fig. 9.** Angular velocity reversal transients of SynRM with signum-based SFC with 3 Nm load torque perturbation for  $i_d^{ref} = 2$  A (left column) and  $i_d^{ref} = -0.5$  A (right column) for  $L_q$  fluctuation: (a) and (d) angular velocity, (b) and (e) direct current, (c) and (f) quadrature current. SynRM, synchronous reluctance motor.

In order to quantify the robustness of the proposed ANN-based G-S SFC, the IAE integral indicator has been analysed for waveforms shown in Figure 7(a) and (d), and Figure 8(a) and (d), respectively. The obtained values are summarised in Table 2.

The obtained results show that the impact of the  $q$ -axis inductance is negligible in both the scenarios considered. In the case of moment of inertia and friction, a higher impact on control system behaviour is observed for  $i_d^{ref} = -0.5$  A, which results in a higher difference in the integral absolute error (IAE) index. It is caused by the higher value of the angular rise time and the much worse load torque compensation. This is in line with the results presented earlier and with expectations, as the dynamics of electromagnetic torque generation is lower in this case, as shown in Figure 6(e) and (j). Regardless of IAE fluctuations, it can be concluded that the proposed control scheme assures good performance and robustness against  $q$ -axis inductance, the moment of inertia and viscous friction, in the investigated ranges.

Finally, the robustness of signum-based SFC has been investigated. As in the case of ANN-based G-S SFC, an impact of  $L_q$ ,  $B_m$  and  $J_m$  fluctuations on the control performance has been analysed, and the obtained results are shown in Figures 9 and 10.

From Figure 9, it can be seen that the robustness of signum-based SFC against  $q$ -axis inductance variation is similar to those observed for ANN-based SFC. By contrast, the overall control performance (e.g. IAE performance index listed in Table 3) is slightly worse for the signum-based approach. A similar conclusion can be drawn from Figure 10, where an investigation against mechanical parameters fluctuation is shown. It should be noted that the

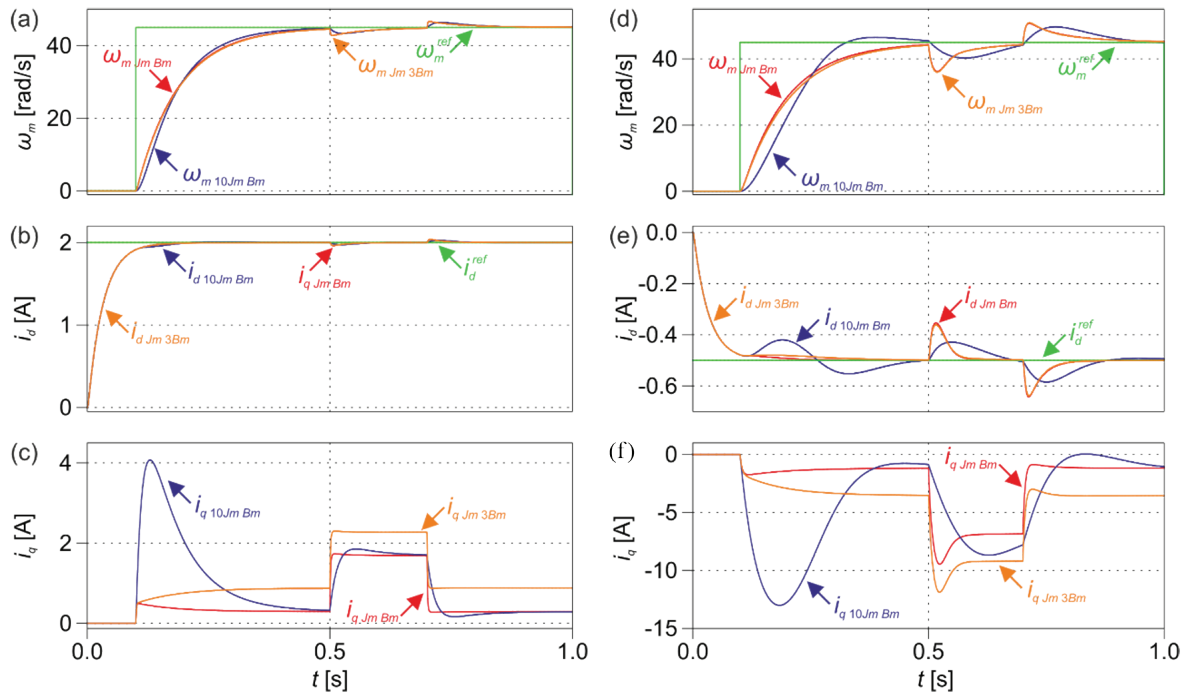


**Fig. 10.** Angular velocity reversal transients of SynRM with signum-based SFC with 3 Nm load torque perturbation for  $i_d^{ref} = 2$  A (left column) and  $i_d^{ref} = -0.5$  A (right column) for  $J_m$  and  $B_m$  fluctuation: (a) and (d) angular velocity, (b) and (e) direct current, (c) and (f) quadrature current. SynRM, synchronous reluctance motor.

**Table 3.** Comparison of the IAE performance index for signum-based SFC for parameters fluctuation

	$L_{q'}, J_m, B_m$	$L_{q'}/2, J_m, B_m$	$2L_{q'}, J_m, B_m$	$L_{q'}, 10J_m, B_m$	$L_{q'}, J_m, 3B_m$
IAE for $i_d^{ref} = 2$ A	4.187	4.173	4.219	4.198	4.248
IAE for $i_d^{ref} = -0.5$ A	5.567	5.517	5.685	6.141	5.811

greater difference in the IAE performance index between ANN-based G-S SFC (Table 2) and signum-based SFC (Table 3) is observed for  $i_d^{ref} = 2$  A. The higher value of the  $d$ -axis current, the greater deviation of the control system from operating conditions are established by the mean value of  $L_d$  (Figure 2(a)) and constant coefficients of SFC (Figure 3).

## 5. Conclusion

In this paper, a G-S SFC has been applied to high-performance control of SynRM with non-linear inductance characteristics. Non-linear coefficients of the G-S SFC are approximated using an ANN. Such a solution assures superior accuracy and relatively low usage of resources during implementation compared with the LUT-based approach. For the sake of comparison, a signum-based SFC has also been developed and investigated. It was proven that applying an augmented drive model with additional state variables assures precise control of angular velocity and  $d$ -axis current in both the considered controllers. The obtained results indicate that the ANN-based G-S SFC assures satisfactory dynamical behaviour of SynRM drive and robustness against  $q$ -axis inductance, the moment of inertia and viscous friction. In the case of signum-based SFC, slightly worse control performance is observed, especially for greater values of the  $d$ -axis current. By contrast, its implementation is much more simplified. Further investigation of the proposed control scheme, including experimental tests, is planned.

## Acknowledgments

This research was supported by the 'Excellence Initiative—Research University' programme of Warsaw University of Technology under grant 'ENERGYTECH-1 Power' and by the 'Excellence Initiative—Research University' programme of Nicolaus Copernicus University.

## References

- Awan, H. A., Saarakkala, S. E. and Hinkkanen, M. (2019). Flux-Linkage-Based Current Control of Saturated Synchronous Motors. *IEEE Transactions on Industry Applications*, 55(5), pp. 4762–4769.
- Bianchi, N., Bolognani, S., Carraro, E., Castiello, M. and Fornasiero, E. (2016). Electric Vehicle Traction Based on Synchronous Reluctance Motors. *IEEE Transactions on Industry Applications*, 52(6), pp. 4762–4769.
- Boldea, I. and Tutelea, L. (2018). *Reluctance Electric Machines: Design and Control*. CRC Press.
- Brasel, M. (2014). A Gain-scheduled Multivariable LQR Controller for Permanent Magnet Synchronous Motor. In: *Proceedings of the 19th International Conference on Methods and Models in Automation and Robotics MMAR, Miedzyzdroje, 2 – 5 September 2014*.
- Credo, A., Fabri, G., Villani, M., and Popescu, M. (2020). Adopting the Topology Optimization in the Design of High-speed Synchronous Reluctance Motors for Electric Vehicles. *IEEE Transactions on Industry Applications*, 56(5), pp. 5429–5438.
- Cvetkovski, G. V. and Petkovska, L. (2021). Selected Nature Inspired Algorithms in Function of PM Synchronous Motor Cogging Torque Minimization. *Power Electronics and Drives*, 6(41), pp. 209–222.
- Ewert, P. (2019). Application of Neural Networks and Axial Flux for the Detection of Stator and Rotor Faults of an Induction Motor. *Power Electronics and Drives*, 4(39), pp. 203–215.
- Grzesiak, L. M. and Tarczewski, T. (2015). *State Feedback Control with ANN Based Load Torque Feedforward for PMSM Fed by 3-Level NPC Inverter with Sinusoidal Output Voltage Waveform*. In: Ferrier J. L., Gusikhin O., Madani K., Sasiadek J., eds., *Informatics in Control, Automation and Robotics. Lecture Notes in Electrical Engineering*, 325, Springer, Cham, pp. 73–90.
- Hadla, H. and Cruz, S. (2016). Active Flux Based Finite Control Set Model Predictive Control of Synchronous Reluctance Motor Drives. In: *Proceedings of the 18th European Conference on Power Electronics and Applications EPE'16 ECCE Europe*, Karlsruhe, 6 – 8 September 2016.
- Hannoun, H., Hilaiet, M. and Marchand, C. (2011). High Performance Current Control of a Switched Reluctance Machine Based on a Gain-Scheduling PI Controller. *Control Engineering Practice*, 19(11), pp. 1377–1386.
- Farhan, A., Abdelrahman, M., Saleh, A., Shaltout, A. and Kennel, R. (2020). Simplified Sensorless Current Predictive Control of Synchronous Reluctance Motor Using On-line Parameter Estimation. *Energies*, 13(2), pp. 1–18.
- Kaźmierkowski, M. P., Blaabjerg, F. and Krishnan, R. (2001). *Control in Power Electronics – Selected Problems*. London: Academic Press.
- Li, J. C., Xin, M., Fan, Z. N. and Liu, R. (2020). Design and Experimental Evaluation of a 12 kW Large Synchronous Reluctance Motor and Control System for Elevator Traction. *IEEE Access*, 8, pp. 34256–34264.
- Lin, F. J., Chen, S. G. and Hsu, C. W. (2018). Intelligent Backstepping Control Using Recurrent Feature Selection Fuzzy Neural Network for Synchronous Reluctance Motor Position Servo Drive System. *IEEE Transactions on Fuzzy Systems*, 27(3), pp. 413–427.
- Lin, F. J., Huang, M. S., Chen, S. G., Hsu, C. W. and Liang, C. H. (2019). Adaptive Backstepping Control for Synchronous Reluctance Motor Based on Intelligent Current Angle Control. *IEEE Transactions on Power Electronics*, 35(7), pp. 7465–7479.
- Oliveira, F. and Ukil, A. (2019). Comparative Performance Analysis of Induction and Synchronous Reluctance Motors in Chiller Systems for Energy Efficient Buildings. *IEEE Transactions on Industrial Informatics*, 15(8), pp. 4384–4393.
- Safonov, M. and Athans, M. (1977). Gain and Phase Margin for Multiloop LQG Regulators. *IEEE Transactions on Automatic Control*, 22(2), pp. 173–179.

- Scalcon, F. P., Osório, C. R., Koch, G. G., Gabbi, T. S., Vieira, R. P., Gründling, H. A., and Montagner, V. F. (2020). Robust Control of Synchronous Reluctance Motors by Means of Linear Matrix Inequalities. *IEEE Transactions on Energy Conversion*, 36(2), pp. 779–788.
- Senjyu, T., Kinjo, K., Urasaki, N. and Uezato, K. (2003). High Efficiency Control of Synchronous Reluctance Motors Using Extended Kalman Filter. *IEEE Transactions on Industrial Electronics*, 50(4), pp. 726–732.
- Shyu, K. K., Lai, C. K. and Hung, J. Y. (2001). Totally Invariant State Feedback Controller for Position Control of Synchronous Reluctance Motor. *IEEE Transactions on Industrial Electronics*, 48(3), pp. 615–624.
- Tarczewski, T. and Grzesiak, L. M. (2009). High Precision Permanent Magnet Synchronous Servo-drive with Lqr Position Controller. *Przegląd Elektrotechniczny*, 85(8), pp. 42–47.
- Tarczewski, T., Niewiara, L. J. and Grzesiak, L. M. (2021). Gain-Scheduled State Feedback Speed Control of Synchronous Reluctance Motor. In: *Proceedings of the 19th International Power Electronics and Motion Control Conference PEMC*, Gliwice, 25–29 April 2021.
- Tarczewski, T., Skiwski, M. and Grzesiak, L. M. (2017). Constrained Non-stationary State Feedback Speed Control of PMSM. In: *Proceedings of the 19th European Conference on Power Electronics and Applications EPE'17 ECCE Europe*, Warsaw, 11–14 September 2017.
- Truong, P. H., Flieller, D., Nguyen, N. K., Mercklé J. and Sturtzer G. (2016). Torque Ripple Minimization in Non-sinusoidal Synchronous Reluctance Motors Based on Artificial Neural Networks. *Electric Power Systems Research*, 140, pp. 37–45.
- Yousefi-Talouki, A., Pescetto, P., Pellegrino, G. and Boldea, I. (2017). Combined Active Flux and High-frequency Injection Methods for Sensorless Direct-flux Vector Control of Synchronous Reluctance Machines. *IEEE Transactions on Power Electronics*, 33(3), pp. 2447–2457.